Manganese–Salicyloximate Clusters Starting from [MnII(hfacac)2]: From Mn4 to Mn12

Albert Escuer*[a] Beatriz Cordero,[a] Mercè Font-Bardia,[b] Simon J. Teat,[c] and Olivier Roubeau[d]

a] Departament de Química Inorgànica and Institut de Nanociencia i Nanotecnologia (IN2UB), Universitat de Barcelona, Av. Diagonal 645, 08028 Barcelona, Spain
E-mail: albert.escuer@ub.edu
http://www.ub.edu/inorgani/recerca/MagMol/magmol.htm
[b] Department de Cristallografia, Mineralogia i Dipòsits Minerals, Universitat de Barcelona, Martí Franquès s/n 08028 Barcelona, Spain
[c] Advanced Light Source, Berkeley Laboratory, 1 Cyclotron Road, Berkeley, CA 94720, USA
[d] Instituto de Ciencia de Materiales de Aragón (ICMA), CSIC-Universidad de Zaragoza, Pl. San Francisco s/n, 50009 Zaragoza, Spain

ABSTRACT:

The systematic exploration of the reactivity of [Mn(hfacac)2] with R-salicyloximes (R-saloxH2: R = H, Me, Et) yielded a family of clusters with nuclearities ranging from Mn4 to Mn12. The compounds with formula [Mn6(O)2(salox)6- (CF3COO)2(EtOH)4] (1) and [Mn12(salox)12(O)4(N3)4(H2O)2-(MeOH)6] (4) show two or four linked {Mn(μ3-O)(salox)3}+ triangular subunits. Magnetic measurements revealed spin ground states of S = 4 for 1 and S = 8 for 4, as well as singlemolecule magnet responses and magnetic hysteresis above 2 K. The cubic [Mn4(Mesalox)4(MesaloxH)4] (2), the hexanuclear [Mn6(Etsalox)6(O)2(MeO)4(MeOH)2] (3) and the octanuclear [Mn8(Mesalox)6(O)2(N3)6(MeOH)8] (5) are polymorphs of previously reported systems. Small structural changes allows an S = 11 ground state for 3.

INTRODUCTION

The discovery of the single-molecule magnet (SMM) response of the hexanuclear complex [Mn6(O)2(salox)6(MeCOO)2] (saloxH2 = salicylaldoxime, Scheme 1) and its benzoate analogue [1] was the starting point for the systematic study of a large family of [Mn6] SMMs exhibiting a wide variety of magnetic responses and spin ground states. These systems are characterized by the hexanuclear core consisting of two {Mn3(O)(oximate)3}+ triangles linked by two η1:η1:η3:μ3 oximate bridges and usually capped by two monovalent anions on the opposite triangular faces. A large number of related hexanuclear clusters have been synthesized by varying the R substituent on the oximate group (R = H,[2] Me,[2c,2g,2j,3] Et,[2b–d,2f,2g,2j,3a,4] Ph,[2j,5] NH2,[6] NMe2,[7] NEt2 [7]). Charge balance in these hexanuclear clusters is achieved usually with coordinated carboxylate anions but in a few cases with other anionic ligands,[2h,2j,3a,6c,6e] cationic clusters being exceptional.[6d] Brechin and co-workers modulated the value of the spin ground state of these hexanuclear cores, reaching the largest possible value of S = 12. On the basis of the experimental data and DFT calculations, the structural features that control the coupling inside the triangular units were elucidated, and it was concluded that the sign of the interaction is dependent on the Mn–N–O–Mn torsion angles, placing the border between ferromagnetic and antiferromagnetic coupling at around 31°.[2c,4c]

Moreover, the ability of R-saloxH2, R-saloxH– and R-salox2– to adopt different coordination modes and their combination with additional donors such as oxo, hydroxo or methoxo have generated a variety of interesting magnetic systems (often with SMM responses), for example, cubanes,[8] Mn5 metallacrowns,[9] bicapped[10] or fused triangles,[11] Mn6 defective cubane[3a] or other topologies,[5,12] Mn7,[13] Mn8,[14] Mn9,[15] Mn12 [16] or even impressive Mn32 rings.[17]

The challenge to enlarge the known topologies and nuclearities derived from manganese and R-saloxH2 ligands lies in the design of new synthetic conditions. The hexafluoroacetylacetonate (hfacac) ligand shows an extremely low affinity for manganese cations in high oxidation states and thus, after the oxidation of [Mn(hfacac)2]/R-saloxH2 mixtures, the intentional lack of coordinating anions could be an approach to stabilizing neutral systems other than the well-known [Mn6] clusters.

Following from this, we have systematically explored the [Mn(hfacac)2]/R-saloxH2 system and its response to the presence of sodium azide. In this work we report the clusters [Mn6(O)2(salox)6(CF3COO)2(EtOH)4]·Et2O (1·Et2O), [Mn4-(Mesalox)4(MesaloxH)4] (2), [Mn6(Etsalox)6(O)2(MeO)4(MeOH)2]· MeOH (3·MeOH), [Mn12(salox)12(O)4(N3)4(H2O)2(MeOH)6]· 4MeOH·2H2O (4·4MeOH·2H2O) and [Mn8(Mesalox)6-(O)2(N3)6(MeOH)8]·4MeOH (5·4MeOH). Complex 1 is a new member of the [Mn6] family of clusters and 4 provides a unique Mn12 topology with SMM response (previously reported in a communication).[16b] Noteworthy, compounds 2, 3 and 5 are polymorphs of the previously reported complexes 2a·3.5MeCN, 3a·MeOH and 5a·10MeOH with different hydrogen-bonding patterns or solvent content, resulting in some cases in drastic differences in their magnetic response.

RESULTS AND DISCUSSION

Structural Description

The charge balance and manganese oxidation states of the metallic atoms of complexes 1–5 were determined from their coordination sphere parameters and the results of bond valence sum (BVS) calculations (Table 1).

[Mn6(O)2(salox)6(CF3COO)2(EtOH)4]·Et2O (1·Et2O)

The centrosymmetric structure of 1 consists of two linked μ3-O-centred triangles (Figure 1). One oximate bridging ligand is placed at each edge of the triangle, two of them in the η1:η1:η1:μ2 mode and the third one in the η2:η1:η1:μ3 mode, linking the axial position of the neighbouring triangle. One synsyn trifluoroacetate ligand, coordinated to each triangular face, and two ethanol molecules coordinated to Mn(3) complete the coordination environment of the triangular units. The bond parameters of 1 (Table 2) are similar to those of other members of the [Mn6] series and therefore only the relevant parameters will be discussed. The torsion angles Mn–N–O–Mn in the triangular units are 4.8(3), 14.2(3) and 21.4(2)°, the larger torsion corresponding to the N(1)–O(3) oxime involved in the η2:η1:η1:μ3 linkage. The inter-triangle Mn(1a)–O(3)–N(1)–Mn(2) torsion angle is 91.1(2)°.
The two ethanol molecules coordinated to Mn(3) allow the formation of intra- and intermolecular hydrogen bonds involving the ethanol molecules and the O atoms of the salox2– ligands: O(11) interacts with O(3a) with an O···O distance of 2.920(3) Å, whereas O(10) interacts with the neighbouring [Mn6] molecule by means of O(10)···O(6) interactions [O···O distance 2.809(3) Å]. These latter hydrogen bonds promote a monodimensional arrangement of hexanuclear complexes linked by double hydrogen bonds (Figure 2).

[Mn4(Mesalox)4(MesaloxH)4] (2)

The molecular structure of the tetranuclear complex 2 is shown in Figure 3 and selected bond parameters are reported in Table 3. The structure of this compound is a polymorph of the 2a·3.5MeCN complex reported by Brechin and co-workers[8a,8c] and is closely related to the chloroform- or methanol-solvated clusters bearing the salicylaldoximato ligand.[8b,8d] The structure consists of four MnIII cations that form a pseudo-cubane cage in which each pentagonal face is defined by one Mn–N–O–Mn and one Mn–O–Mn linkage. Each MnIII cation links one MesaloxH–and one Mesalox2– ligand and exhibits a hexacoordinated environment. The bond parameters inside the cage are very similar to those reported for the complex 2a and will not be further discussed.

[Mn6(Etsalox)6(O)2(MeO)4(MeOH)2]·MeOH (3·MeOH)

The mixed-valent MnIII 4MnIV 2 hexanuclear complex 3 is also a polymorph of the 3a·MeOH complex reported by Brechin and co-workers.[3a] A plot of the structure is shown in Figure 4 and some selected bond parameters are reported in Table 4. The complex can be described as two μ3-O(1)-centred MnIII 2MnIV triangles linked exclusively through the trivalent metallic atoms by four methoxo bridges. Each triangular subunit contains three η1:η1:η1:μ2 Etsalox2– ligands, two of them linked to the tetravalent Mn(1) atom and the third one to Mn(3). The Mn(2) cation completes its MnO6 coordination sphere with six O atoms from bridging oxime, methoxo and oxo ligands. The methanol solvate molecule is linked by means of two hydrogen bonds to the coordinated O atoms of one methanol ligand and one salicyl group with O(10)···O(1w) and O(1w)···O(6) distances of 2.550(5) and 2.823(5) Å, respectively. Intermolecular hydrogen bonds were not found. The main difference between 3 and the 3a·MeOH polymorph reported by Brechin and co-workers lies in the hydrogen bonds promoted by the solvate methanol molecules, which in that case involves only O-phenolic atoms. As will be discussed in the magnetic section, these small structural changes modify drastically its magnetic response.

[Mn12(salox)12(O)4(N3)4(H2O)2(MeOH)6]·4MeOH·2H2O (4)

A partially labelled plot of the centrosymmetric structure of 4 is shown in Figure 5 and the main bond parameters are listed in Table 5. The structure contains 12 MnIII cations as a result of the linkage of four {Mn3(μ3-O)(salox)3}+ subunits giving the [MnIII 12(μ3-O)4(μ-N3)4(μ-OR)4]20+ core. Eight salox2– ligands show the η1:η1:η1:μ2 coordination mode linking two MnIII ions in the triangles whereas four salox2– ligands in the η2:η1:η1:μ3 coordination mode form inter-triangle bridges. Four end-on azido bridges complete the linkage between the central Mn6 unit and the external triangles. The inner triangles [Mn(1,2,3) and symmetry related, bridged by the oximato oxygen atoms O7 and O7′] give a fragment fully comparable to the classical [Mn6] core and thus the structure can be described as a [Mn6] cluster bicapped by two [Mn3] triangles.

The Mn–N–Mn bond angles involving the azido bridges, that is, Mn(1)–N(4)–Mn(4) and Mn(3)–N(7)–Mn(5), are relatively large with values of 131.87(8) and 126.76(8)°, respectively. The Mn– N–O–Mn torsion angles are 13.4(2), 16.9(2) and 33.2(2)° for the Mn(1,2,3) inner triangles and 12.0(2), 23.1(2) and 38.5(1)° for the Mn(4,5,6) external triangles. The Jahn–Teller elongation axes of the MnIII ions are roughly perpendicular to the main planes of the triangles in all cases. The azido bridges promote a larger intermetallic distance than the oximato bridge and as consequence the mean planes defined by the Mn(1,2,3) and Mn(4,5,6) atoms are tilted at 41.38(1)°.

The coordinated water molecules, methanol and the crystallisation solvent molecules and O salox atoms promote intra- and intermolecular hydrogen bonds. Intramolecular hydrogen bonds link the methanol molecule coordinated to Mn(6) with one azido ligand [O(17)···N(7) distance 2.804 Å], whereas the solvate methanol molecules form several hydrogen bonds with the methanol molecules coordinated to Mn(5), Mn(6) and the μ3-O(9) atom.

The most relevant intermolecular interactions are the double hydrogen bonds established between the water molecule coordinated to Mn(6) and the O-phenoxo atom of the neighbouring [Mn12] cluster [also coordinated to the Mn(6′) atom] with an O(14)···O(18′) distance of 2.764(2) Å, which leads to a chain of [Mn12] clusters (Figure 6).

[Mn8(Mesalox)6(O)2(N3)6(MeOH)8]·4MeOH (5·4MeOH)

The octanuclear mixed-valent MnII 2MnIII 6 complex 5 is a polymorph of the 5a·10MeOH complex reported by Brechin and coworkers.[14] A plot of the asymmetric unit is shown in Figure 7 and the main bond parameters are summarized in Table 6. The system consists of a [Mn6] cluster capped by two {MnII(MeOH)3} fragments that are linked to the corresponding triangles by means of three end-on azido bridges with large MnII–N–MnIII bond angles in the range 117.0–119.4°. The Mn–N–O–Mn torsion angles show values in the range 35.3–42.3°.

The μ3-O atom is located exactly in the Mn3 main plane and consequently the Mn–O(4)–Mn bond angles are very close to 120°. The Mn(2) cation shows a square-pyramidal environment, weakly interacting with the phenoxo O(9′) atom of the neighbouring triangle. The remaining bond parameters and general shape are close to those of the previously reported analogous complex, the main differences lying in the inter-cluster interactions mediated by the methanol molecules in 5. The interaction between N(3) of one azide ligand and O(2) from a coordinated molecule of methanol in a neighbouring molecule leads to 2D chains of clusters (Figure 7).

Comments on the Syntheses

Analysis of the structural data of the neutral [Mn6]2+ clusters reported until now shows that monovalent anions acting as monodentate ligands (carboxylates and halides) or bidentate ligands (typically syn-syn carboxylates) help to stabilize the neutral clusters through links to opposite triangular faces occupying the axial coordination sites. The target of this work was to try to obtain related new topologies by suppressing the axialcoordinated anions, that is, by the synthesis of clusters without participation of the anions of the starting MnIIX2 salts. The hexafluoroacetylacetonate ligand is a well-known ligand in MnII chemistry whereas its coordination to MnIII,IV cations is strongly unfavoured. Therefore, starting from [Mn(hfacac)2] and after the oxidation of the manganese atoms, we can dispose of a reaction medium without anions other than the R-saloxH– or Rsalox2– ligands and eventually the added azide anion or oxo, hydroxo or alkoxo ligands generated by the basic medium. The reactions of R-saloxH2 and [Mn(hfacac)2] effectively generated the neutral complexes 2 (containing only anionic MesaloxH– and Mesalox2–) and 3 (containing only anionic Etsalox2–, methoxo and oxo ligands). Under the same conditions we also obtained complex 1, which shows the typical [Mn6] core capped by trifluoroacetate anions. The formation of the trifluoroacetate anions is not surprising because it is well known that retro-Claisen condensation reactions of β-diketones produce the ketone and the corresponding carboxylate in

basic medium.[18] Thus, the formation in good yield of pure compound 1 indicates extensive and rapid breaking of the hfacac–reagent.

In the light of these results, our strategy was to combine [Mn(hfacac)2] and R-saloxH2 with sodium azide in the reaction medium. If the coordination of hfacac– is excluded, the potentially bridging azido ligand becomes the only available anion in solution and the possibility of obtaining azido-linked [Mn6] cages or other topologies may be favoured. This strategy yielded the [Mn12] complex 4 consisting of four oximate/azidolinked triangular subunits and the octanuclear system 5, which can be envisaged as a [Mn6] cage bicapped by additional MnII ions involving in the two cases end-on azido bridges.

The apparently simple [Mn(hfacac)2]/R-saloxH2 and [Mn(hfacac)2]/R-saloxH2/NaN3 mixtures result in a complicated set of interlocked reactions, summarized in Scheme 2, which are more complicated than the conventional "one-pot" reaction that usually only yields one stable compound. The reaction of saloxH2 with [Mn(hfacac)2] yields only compound 1 containing trifluoroacetate anions. The same reaction in the presence of sodium azide gives the dodecanuclear complex 4 but if the solution containing crystals of 4 is left undisturbed for some weeks, the crystals of the [Mn12] complex slowly redissolve and big crystals of complex 1 can be collected. In contrast, the analogous [Mn(hfacac)2]/R-saloxH2 (R = Me, Et) reactions produce complexes 2 and 3 without the presence of trifluoroacetate. More surprising was the reaction of MesaloxH2 with [Mn(hfacac)2] in the presence of sodium azide, which initially yields pure tetranuclear complex 2 (without coordinated azide) as well-formed crystals in 1–2 days. If the solution is left undisturbed to crystallize for some additional days, the crystals of 2 redissolve and then the pure octanuclear complex 5 (containing azido bridges) starts to crystallize (Scheme 2).

It should be emphasized that complexes 2, 3·MeOH and 5·4MeOH are pseudo-polymorphs of the previously reported clusters 2a·3.5MeCN, 3a·MeOH and 5a·10MeOH, respectively. Although the structural parameters of the cluster cores are very similar, they crystallize in different space groups and the hydrogen bonds promoted by the solvents are also logically different. As is described below, the magnetic responses of 2 and 5 are similar to those reported for their polymorphs whereas for compound 3·MeOH the magnetic response is drastically different.

Magnetic Measurements and Modelling

The room-temperature MT value for compound 1 is 15.73 cm3 mol–1 K, lower than the expected value for six S = 2 centres (18.0 cm3 mol–1 K). On cooling, the MT product gradually decreases down to 15 K (5.89 cm3 mol–1 K). Below this temperature the MT product abruptly decreases, tending to zero at low temperatures (Figure 8). The M plot exhibits a maximum susceptibility at 4 K (Figure 8, inset). The susceptibility plot clearly shows two kinds of interactions: in the 300–15 K range, the observed decay of the MT product corresponds to intracluster coupling, whereas the low-temperature region reflects strong intercluster interactions mediated by the double hydrogen bonds involving Mn(3) (Figure 2). Both isolated clusters and systems in which the [Mn6] units are connected by hydrogen

bonds involving coordinated and crystallization solvent molecules exhibit a minimum at around 20–25 K or small decays of MT below this temperature. In contrast, compound 1 provides an unusual case of strong 1D intercluster interactions that lead to a collapse of the local [Mn6] S = 4 spins for the whole solid. Thus, the experimental susceptibility data for the two kinds of interactions have been analysed separately.

The experimental data for the intracluster interactions were fitted in the 25–300 K range by using the PHI program[19] on the basis of the coupling pattern shown in Scheme 3 (A). Previous fits taking into account all the coupling constants applying the Hamiltonian in Equation (1)

$$H = -J1(S1S4) - J2(S1S3 + S4S6) - J3(S2S3 + S5S6) - J4(S1S2 + S4S5) - J5(S3S4 + S1S6) \quad (1)$$

show a negligible value for J5 and similar values of –11.7 and –13.0 cm–1 for J3 and J4. In the light of this result we decided to fit the system by using the simplified 3-J Hamiltonian in Equation (2)

$$H = -J1(S1S4) - J2(S1S3 + S4S6) - J3(S2S3 + S5S6 + S1S2 + S4S5) \quad (2)$$

in which we have assumed that J5 = 0 in Equation (1) and that there are only two coupling constants inside the triangles (Scheme 3, B). The best-fit parameters were J1 = +14.8 cm–1, J2 = –5.5 cm–1, J3 = J4 = –13.0 cm–1 and g = 2.063. The antiferromagnetic (AF) interactions inside the triangular units (negative values for J2, J3 and J4) are in good agreement with the Mn–O–N–Mn torsion angles, clearly below the ferro/anti-ferromagnetic border of 31° and thus the spin ground state for complex 1 is the conventional S = 4.

Magnetization experiments performed in an external field up to 5 T show a sigmoid shape of the magnetization plot and an unsaturated value equivalent to only six electrons under high field (Figure 9). The first derivative of the magnetization plot shows a maximum at around 1.1 T and therefore the intercluster interaction can be evaluated to be approximately 1 cm–1.

As was expected from the strong intercluster interactions, ac susceptibility measurements did not show complete out-ofphase peaks and only very weak tails of the M″ signals were observable.

The room-temperature MT value for compound 2 is 12.17 cm3 mol–1 K, close to the expected value of 12.0 cm3 mol–1 K for four non-interacting S = 2 spins (Figure 10). On cooling, the value of MT increases monotonically up to a maximum of 26.8 cm3 mol–1 K at 4 K, which suggests ferromagnetic interacttions and a spin ground state of S = 8. The experimental data were fitted by applying the Hamiltonian in Equation (3) derived from the coupling pattern in Scheme 3 (C) assuming J1 = J2 to compare with the fit of its pseudo-polymorph 2a·3.5MeCN.

$$H = -J1(S1S2 + S2S4 + S4S3 + S3S1 + S1S4 + S2S3) \quad (3)$$

The best fit of the experimental data gives J = + 0.8 cm–1 and g = 1.96, in agreement with the values reported for compound 2a and its Etsalox2– analogue.[8a] The magnetization data and the tails of the out-of phase signal found in the ac measurements are also very similar to those of compound 2·3.5MeCN and will not further be discussed.

The room-temperature MT value for compound 3 is 16.02 cm3 mol–1 K, slightly larger than the expected value for four S = 2 and two S = 3/2 centres (15.75 cm3 mol–1 K; Figure 10). On cooling, MT increases continuously up to a maximum value of 71.07 cm3 mol–1 K at 2 K. The continuous increase of MT and its value at low temperature suggest a fully ferromagnetic coupling with a spin ground state of S = 11. The coupling pattern of interactions for 3 shows nine super-exchange pathways mediated by different kinds of bridges, which implies five J coupling constants. The fit of the experimental data in the 300–10 K range applying the Hamiltonian in Equation (4)

$$H = -J1(S5S6) - J2(S3S6 + S4S5) - J3(S3S5 + S4S6) - J4(S1S5 + S2S6) - J5(S1S3 + S2S4) \quad (4)$$

fast saturation of the magnetization with a final quasi-saturated value equivalent to 20.6 electrons under the maximum external field, which is very close to the proposed S = 11. The magnetization plot for S = 11 gives an excellent fit for the parameters D = +0.24 cm–1 and g = 2.00 (Figure 10, inset). The easy-axes of the MnIII ions are far from parallel and are directed towards the μ3-OMe donors. This unfavourable arrangement of the easy-axesand the positive sign of D preclude an SMM response and effectively AC experiments do not show any out-of-phase signals.

Our results indicate a higher ground state than that obtained for the polymorph 3a previously reported by Brechin and coworkers. In that case the MT plot increased continuously from the lower value of 14.4 cm3 mol–1 K up to a maximum value of 23.49 cm3 mol–1 K with a proposed spin ground state of S = 6. The modelling of 3a was unsuccessful. The reason for the different magnetic responses cannot be attributed to the Mn–O–Mn bond angles, which are identical within the margin of error of ±1°. In contrast, the subtle differences induced by the hydrogen bonds become important for the most easily deformable Mn–N–O–Mn torsion angles, the MnIV(1)–O(3)–N(1)–MnIII(3) torsion being the most significant, increasing from 34.3° in the case of 3a to 47.0(1)° for 3.

The magnetic response of compound 4 was discussed in depth in the previous communication[16b] and thus only a brief description will be given here. The room-temperature MT value for compound 4 is 31.8 cm3 K mol–1, slightly lower than the expected value for 12 non-interacting S = 2 spins (36.0 cm3 K mol–1; Figure 10). On decreasing the temperature the value of MT decreases continuously with a higher rate of decay below 15 K, probably due to intermolecular hydrogen bonds, with a value of 6.8 cm3 K mol–1 at low temperature. The large number of interactions and the size of 4 exclude a conventional fit of the experimental data. However, an analysis of its structural parameters permits a good estimation of its magnetic response. The Mn–N–O–Mn torsion angles in the triangular subunits are

quite similar with values of 13.4, 16.9 and 33.2° for the Mn(1,2,3) triangles and 12.0, 23.1 and 38.5° for the Mn(4,5,6) triangles. According to the well-stablished rules for these kinds of systems,[2c,4c] a local S = 2 should be expected for all the triangular subunits. For a centrosymmetric compound such as 4, the only possibilities for describing the inter-triangle interactions are AF/AF/AF, AF/FM/AF, FM/AF/FM or FM/FM/FM. All combinations containing at least one AF interaction lead to an S = 0 ground state, which is incompatible with the experimental data, whereas ferromagnetic interactions between the triangles give an S = 8 spin ground state as the only possibility.

Magnetization experiments showed a quasi-saturated value of around 12 electrons under an external field of 5 T, which is compatible with an anisotropic S = 8 ground state. The fit of the reduced magnetization did not give consistent results due to the effect of the intermolecular hydrogen bonds and the low-lying excited states. However, the large gaps between the magnetization plots unambiguously suggest a relatively large anisotropic ground state. The ac measurements under an oscillating field of 4 G were performed in the frequency range 1300–50 Hz (Figure 11), and out-of-phase frequency-dependent signal were found with maxima in the 4.09–3.47 K range. A fit to was satisfactory for the values of J1 = +4.2 cm–1, J2 = +4.8 cm–1, J3 = +2.0 cm–1, J4 = +5.8 cm–1, J5 = +3.2 cm–1 and g = 1.97. Equally satisfactory was the fit assuming only three J coupling constants, one for the double methoxo bridges between MnIII atoms (J1 = J2), one for the oxo-methoxo bridges between the MnIII atoms (J3) and finally a common J4 = J5 for the four interactions between MnIII/MnIV centres. Under these conditions the best-fit values of J1 = J2 = +4.6 cm–1, J3 = +2.0 cm–1, J4 = J5 = +4.4 cm–1 and g = 1.98 were obtained. The coupling constants calculated for a ferromagnetic system with such a large number of interactions is poorly reliable but the magnitudes and signs of the constants indicate a moderately ferromagnetic (FM) system supporting the maximum S = 11 spin ground state. This assumption was also confirmed by the magnetization experiment performed up to 5 T, which showed the characteristic the Arrhenius equation gives an Ueff value of 51 cm–1 and a D value of 0.80 cm–1 assuming S = 8. The magnetization hysteresis cycle measured with a coercive field of around 1000 G at 2 K confirmed SMM behaviour with a blocking temperature T greater than 2 K (Figure 11, inset).

The room-temperature MT value for compound 5 is 20.38 cm3 mol–1 K, lower than the expected value for six S = 2 and two S = 5/2 centres (26.75 cm3 mol–1 K; Figure 10). On cooling, the MT plot decreases to a minimum value of 14.64 cm3 mol–1 K at 25 K and then increases up to a maximum value of 16.21 cm3 mol–1 K at 7 K. This shape is characteristic of ferrimagnetic interactions resulting from ferromagnetic interactions inside the MnIII 6 core with the three Mn–N–O–Mn torsion angles clearly larger than 31° (local spin for the Mn6 unit S = 12) and the anti-ferromagnetic coupling with the two MnII cations mediated by the MnII–N–MnIII bond angles,[20] resulting in the ground state S = 12 – 5/2 – 5/2 = 7. The shape and values of the MT plot and the magnetization data are in agreement with its polymorph 5a and will not be discussed further.

CONCLUSIONS

The reactions of [Mn(hfacac)2] with R-saloxH2 ligands (R = H, Me, Et) have yielded five clusters MnIII6 (1), MnIII4 (2), MnIII4MnIV2(3), MnIII12 (4) and MnII2MnIII6 (5). Some of them are new compounds, such as 1 and 4, whereas 2, 3 and 5 are polymorphs of previously reported systems. As expected, the hfacac ligands do not participate in the final complexes with high-valent manganese atoms, but they can play a role after solvolysis, as in complex 1, which contains CF3COO– anions. Dodecanuclear complex 4 is an example of this synthetic strategy, exhibiting a SMM response and a large energy barrier of magnetization. Complex 3 is a good example of how small structural changes can modify the spin ground state, in this case reaching the maximum value S = 11.

EXPERIMENTAL SECTION

Physical Measurements: Magnetic susceptibility measurements were carried out on polycrystalline samples with a MPMS5 Quantum Design susceptometer in the range 30–300 K at a magnetic field of 0.3 T and in the range 30–2 K at a field of 0.03 T to avoid saturation effects at low temperatures. Diamagnetic corrections were estimated from Pascal Tables. IR spectra (4000–400 cm–1) were recorded in KBr pellets with a Bruker IFS-125 FT-IR spectrophotometer.

Syntheses: [Mn(hfacac)2] and saloxH2 ligand were purchased from Sigma–Aldrich Inc. and used without further purification. MesaloxH2 and EtsaloxH2 were prepared following previously reported methods.[21]

Synthesis of [Mn6(O)2(salox)6(CF3COO)2(EtOH)4]·Et2O (1·Et2O), [Mn4(Mesalox)4(MesaloxH)4] (2), [Mn6(Etsalox)6(O)2(MeO)4-(MeOH)2]·MeOH (3·MeOH), [Mn12(salox)12(O)4(N3)4(H2O)2-(MeOH)6]·4MeOH·2H2O (4·4MeOH·2H2O) and [Mn8(Mesalox)6-(O)2(N3)6(MeOH)8]·4MeOH (5·4MeOH): Specific synthetic conditions are summarized in Table 7. The five complexes were synthesized following very similar experimental procedures. The R-salicyloxime ligand (1 mmol) and the appropriate base (1 mmol) were added to a solution of [Mn(hfacac)2] (0.526 g, 1 mmol) in the corresponding solvent (20 mL). For 4 and 5, sodium azide (0.63 g, 1 mmol) was also added. The mixtures were stirred for 30 min in the open air and the resulting dark-green solutions were filtered. Well-formed dark-green crystals were obtained in yields of around 40 % after a few days of layering the final solutions with diethyl ether. These crystals were employed for the instrumental measurements. As mentioned above, if after the crystallization of 2 and 4 their solutions were left undisturbed, they evolved to compounds 5 and 1, respectively.

C54H54F6Mn6N6O22 (1): calcd. C 40.98, H 3.44, N 5.31; found C 39.4, H 3.6, N 5.1.

C64H60Mn4N8O16 (2): calcd. C 54.25, H 4.27, N 7.91; found C 53.8, H 4.3, N 7.8.

C61H78Mn6N6O21 (3): calcd. C 46.94, H 5.04, N 5.38; found C 47.3, H 4.9, N 5.2.

C94H108Mn12N24O42 (4): calcd. C 38.86, H 3.75, N 11.57; found C 39.3, H 3.64, N 11.2.

C60H90Mn8N24O26 (5): calcd. C 35.97, H 4.52, N 16.78; found C 36.4, H 4.2, N 17.2.

Intense IR bands (KBr): 1: ν˜ = 1654, 1599, 1584, 1542, 1441, 1327, 1201, 1149, 1028, 918, 681, 466 cm–1; 2: ν˜ = 1597, 1435, 1310, 1290, 972, 783, 667, 645, 682, 616 cm–1; 3: ν˜ = 1593, 1565, 1435, 1305, 1139, 1095, 1004, 942, 754, 680, 542 cm–1; 4: ν˜ = 2056, 1598, 1539, 1439, 1286, 1203, 1029, 916, 753, 668 cm–1; 1: ν˜ = 2069, 1596, 1436, 1304, 1233, 1042, 961, 861, 683 cm–1.

Single-Crystal X-ray Structure Analyses: Data for compounds 2, 4 and 5 were collected with a Bruker APEX II CCD diffractometer on Advanced Light Source beam line 11.3.1 at Lawrence Berkeley National Laboratory using a silicon 111 monochromator (T = 100 K, λ = 0.7749 Å). The structures were solved by direct methods and the refinement on F2 and all further calculations were carried out by using the SHELXTL suite.[22] All non-hydrogens were refined anisotropically. Hydrogen atoms were refined

by placing them geometrically on their carrier atom and using a riding model except in the cases of 4 and 5. In 4 the hydrogen atoms of the water molecules and of the hydroxy groups of the methanol molecules, both coordinated and in the lattice, were found in a difference Fourier map and refined freely with their thermal parameter 1.5 times that of their carrier oxygen and a distance restraint. In 5 the hydrogen atoms on the coordinated methanol molecules (O1, O2, O3, O11) could not be found in difference Fourier maps nor fixed and are thus not included in the structural model.

Data for compounds 1 and 3 were collected with a MAR345 diffractometer using an image plate detector. The structures were solved by direct methods using the SHELXS computer program and refined by full-matrix least-squares methods with SHELX97 computer program.[23] Two hydrogen atoms were located from a difference synthesis in 3 and all hydrogen atoms were computed and refined by using a riding model with an isotropic temperature factor equal to 1.2 times the equivalent temperature factor of the atom to which they are linked.

The crystallographic details for 1–5 are summarized in Table 8.

CCDC 1438011 (for 1), 1438012 (for 2), 1438013 (for 3), 804307 (for 4), and 1438014 (for 5) contain the supplementary crystallographic data for this paper. These data can be obtained free of charge from The Cambridge Crystallographic Data Centre.

ACKNOWLEDGMENTS

This work was supported by the Centro de Investigación Científica y Tecnológica (CICYT) (project number CTQ2015-63614-P). The Advanced Light Source is supported by the Director, Office of Science, Office of Basic Energy Sciences of the U.S. Department of Energy (contract number DE-AC02-05CH11231).

Keywords: Cluster compounds · Magnetic properties · Manganese · N,O ligands

[1] C. J. Milios, C. P. Raptopoulou, A. Terzis, F. Lloret, R. Vicente, S. P. Perlepes, A. Escuer, Angew. Chem. Int. Ed. 2004, 43, 210–212; Angew. Chem. 2004, 116, 212.

[2] a) C. J. Milios, A. Vinslava, A. G. Whittaker, S. Parsons, W. Wernsdorfer, G. Christou, S. P. Perlepes, E. K. Brechin, Inorg. Chem. 2006, 45, 5272–5274; b) C. J. Milios, A. Vinslava, W. Wernsdorfer, A. Prescimone, P. A. Wood, S. Parsons, S. P. Perlepes, G. Christou, E. K. Brechin, J. Am. Chem. Soc. 2007, 129, 6547–6561; c) C. J. Milios, R. Inglis, A. Vinslava, R. Bagai, W. Wernsdorfer, S. Parsons, S. P. Perlepes, G. Christou, E. K. Brechin, J. Am. Chem. Soc. 2007, 129, 12505–12511; d) L. F. Jones, C. J. Milios, A. Prescimone, M. Evangelisti, E. K. Brechin, C. R. Chim. 2008, 11, 1175–1181; e) C. P. Raptopoulou, A. K. Boudalis, K. N. Lazarou, V. Psycharis, N. Panopoulos, M. Fardis, G. Diamantopoulos, J. P. Tuchagues, A. Mari, G. Papavassiliou, Polyhedron 2008, 27, 3575–3586; f) F. Moro, V. Corradini, M. Evangelisti, V. De Renzi, R. Biagi, U. del Pennino, C. J. Milios, L. F. Jones, E. K. Brechin, J. Phys. Chem. B 2008, 112, 9729–9735; g) R. Inglis, L. F. Jones, C. J. Milios, S. Datta, A. Collins, S. Parsons, W. Wernsdorfer, S. Hill, S. P. Perlepes, S. Piligkos, E. K. Brechin, Dalton Trans. 2009, 3403–3412; h) C.-I. Yang, K.-H. Cheng, M. Nakano, G.-H. Lee, H.-L. Tsai, Polyhedron 2009, 28, 1842–1851; i) X. Song, R. Liu, S. Zhang, L. Li, Inorg. Chem. Commun. 2010, 13, 828–830; j) R. Inglis, S. J. Dalgarno, E. K. Brechin, Dalton Trans. 2010, 39, 4826–4831; k) X.-T. Liu, J.-X. Li, X. Fei, Q.-L. Wu, B. Yang, Chin. J. Inorg. Chem. 2012, 28, 1234–1238; l) G. Novitchi, G. Pilet, D. Luneau, C. R. Chim. 2012, 15, 937–942; m) M. Holynska, S. Dehnen, Z. Anorg. Allg. Chem. 2012, 638, 763–769.

[3] a) L. F. Jones, R. Inglis, M. E. Cochrane, K. Mason, A. Collins, S. Parsons, S. P. Perlepes, E. K. Brechin, Dalton Trans. 2008, 6205–6210; b) C.-L. Zhou, Z.-M. Wang, B.-W. Wang, S. Gao, Polyhedron 2011, 30, 3279–3283.

[4] a) C. J. Milios, A. Vinslava, P. A. Wood, S. Parsons, W. Wernsdorfer, G. Christou, S. P. Perlepes, E. K. Brechin, J. Am. Chem. Soc. 2007, 129, 8–9; b) C. J. Milios, A. Vinslava, W. Wernsdorfer, S. Moggach, S. Parsons, S. P. Perlepes, G. Christou, E. K. Brechin, J. Am. Chem. Soc. 2007, 129, 2754–2755; c) C. J. Milios, R. Inglis, R. Bagai, W. Wernsdorfer, A. Collins, S. Moggach, S. Parsons, S. P. Perlepes, G. Christou, E. K. Brechin, Chem. Commun. 2007, 3476–3478; d) A. Prescimone, C. J. Milios, S. Moggach, J. E. Warren, A. R. Lennie, J. Sanchez-Benitez, K. Kamenev, R. Bircher, M. Murrie, S. Parsons, E. K. Brechin, Angew. Chem. Int. Ed. 2008, 47, 2828–2831; Angew. Chem. 2008, 120, 2870; e) L. F. Jones, M. E. Cochrane, B. D. Koivisto, D. A. Leigh, S. P. Perlepes, W. Wernsdorfer, E. K. Brechin, Inorg. Chim. Acta 2008, 361, 3420–3426; f) A. Prescimone, C. J. Milios, J. Sanchez-Benitez, K. V. Kamenev, C. Loose, J. Kortus, S. Moggach, M. Murrie, J. E. Warren, A. R. Lennie, S. Parsons, E. K. Brechin, Dalton Trans. 2009, 4858–4867.

[5] V. Kotzabasaki, R. Inglis, M. Siczek, T. Lis, E. K. Brechin, C. J. Milios, Dalton Trans. 2011, 40, 1693–1699.

[6] a) A. R. Tomsa, J. Martínez-Lillo, Y. Li, L. M. Chamoreau, K. Boubekeur, F. Farias, M. A. Novak, E. Cremades, E. Ruiz, A. Proust, M. Verdaguer, P. Gouzerh, Chem. Commun. 2010, 46, 5106–5108; b) G.-Y. An, A.-L. Cui, H.-Z. Kou, Inorg. Chem. Commun. 2011, 14, 1475; c) J. Martínez-Lillo, A. R. Tomsa, Y. Li, L. M. Chamoreau, E. Cremades, E. Ruiz, A. L. Barra, A. Proust, M. Verdaguer, P. Gouzerh, Dalton Trans. 2012, 41, 13668–13681; d) J. Martínez-Lillo, N. Dolan, E. K. Brechin, Dalton Trans. 2013, 42, 12824–12827; e) J. Martínez-Lillo, N. Dolan, E. K. Brechin, Dalton Trans. 2014, 43, 4408–4414.

[7] J. Martínez-Lillo, L. M. Chamoreau, A. Proust, M. Verdaguer, P. Gouzerh, C. R. Chim. 2012, 15, 889–894.

[8] a) C. J. Milios, A. Prescimone, A. Mishra, S. Parsons, W. Wernsdorfer, G. Christou, S. P. Perlepes, E. K. Brechin, Chem. Commun. 2007, 153–155; b) A. S. Kumbhar, M. P. Mulay, S. B. Padhye, S. S. Tavale, V. G. Puranik, Struct. Chem. 2008, 19, 735–740; c) R. Inglis, C. C. Stoumpos, A. Prescimone, M. Siczek, T. Lis, W. Wernsdorfer, E. K. Brechin, C. J. Milios, Dalton Trans. 2010, 39, 4777–4785; d) M. Holynska, C. Pietzonka, S. Dehnen, Z. Anorg. Allg. Chem. 2011, 637, 556–561.

[9] a) M. S. Lah, V. L. Pecoraro, J. Am. Chem. Soc. 1989, 111, 7258–7259; b) C. Dendrinou-Samara, A. N. Papadopoulos, D. A. Malamatari, A. Tarushi, C. P. Raptopoulou, A. Terzis, E. Samaras, D. P. Kessissoglou, J. Inorg. Biochem. 2005, 99, 864–875.

[10] a) C.-I. Yang, W. Wernsdorfer, G.-H. Lee, H.-L. Tsai, J. Am. Chem. Soc. 2007, 129, 456–457; b) P. L. Feng, C. J. Stephenson, A. Amjad, G. Ogawa, E. del Barco, D. N. Hendrickson, Inorg. Chem. 2010, 49, 1304–1306.

[11] a) C. Kozoni, M. Siczek, T. Lis, E. K. Brechin, C. J. Milios, Dalton Trans. 2009, 9117–9119; b) C. Kozoni, E. Manolopoulou, M. Siczek, T. Lis, E. K. Brechin, C. J. Milios, Dalton Trans. 2010, 39, 7943–7950.

[12] a) D. P. Kessissoglou, J. Kampf, V. L. Pecoraro, Polyhedron 1994, 13, 1379–1391; b) C. Dendrinou-Samara, G. Psomas, L. Iordanidis, V. Tangoulis, D. P. Kessissoglou, Chem. Eur. J. 2001, 7, 5041–5051; c) C. Dendrinou-Samara, L. Alevizopoulou, L. Iordanidis, E. Samaras, D. P. Kessissoglou, J. Inorg. Biochem. 2002, 89, 89–96; d) J.-P. Geng, Z.-X. Wang, M.-X. Li, H.-P. Xiao, Polyhedron 2011, 30, 3134–3136; e) B. R. Tigyer, M. Zeller, C. M. Zaleski, Acta Crystallogr., Sect. E: Struct. Rep. Online 2011, 67, m1041–u468; f) B. R. Tigyer, M. Zeller, C. M. Zaleski, Acta Crystallogr., Sect. E: Struct. Rep. Online 2012, 68, m1521–m1522; g) K. Mason, J. Chang, A. Prescimone, E. Garlatti, S. Carretta, P. A. Tasker, E. K. Brechin, Dalton Trans. 2012, 41, 8777–8785; h) B. R. Tigyer, M. Zeller, C. M. Zaleski, Acta Crystallogr., Sect. E: Struct. Rep. Online 2013, 69, m393–m394; i) J. C. Lutter, J. W. Kampf, M. Zeller, C. M. Zaleski, Acta Crystallogr., Sect. E: Struct. Rep. Online 2013, 69, m483–m484.

[13] C. J. Milios, I. A. Gass, A. Vinslava, L. Budd, S. Parsons, W. Wernsdorfer, S. P. Perlepes, G. Christou, E. K. Brechin, Inorg. Chem. 2007, 46, 6215–6217.

[14] a) C. J. Milios, R. Inglis, A. Vinslava, A. Prescimone, S. Parsons, S. P. Perlepes, G. Christou, E. K. Brechin, Chem. Commun. 2007, 2738–2740; b) C. J. Milios, R. Inglis, L. F. Jones, A. Prescimone, S. Parsons, W. Wernsdorfer, E. K. Brechin, Dalton Trans. 2009, 2812–2822.

[15] a) R. Inglis, F. White, S. Piligkos, W. Wernsdorfer, E. K. Brechin, G. S. Papaefstathiou, Chem. Commun. 2011, 47, 3090–3092; b) M. Holynska, N. Frank, C. Pichon, I.-R. Jeon, R. Clérac, S. Dehnen, Inorg. Chem. 2013, 52, 7317–7319; c) S. Wang, L. Kong, H. Yang, Z. He, Z. Jiang, D. Li, S. Zeng, M. Niu, Y. Song, J. Dou, Inorg. Chem. 2011, 50, 2705–2707.

[16] a) M.-H. Liu, C.-I. Yang, G.-H. Lee, H.-L. Tsai, Inorg. Chem. Commun. 2011, 14, 1136–1139; b) B. Cordero, O. Roubeau, S. J. Teat, A. Escuer, Dalton Trans. 2011, 40, 7127–7129; c) M. Holynska, R. Clérac, S. Dehnen, Eur. J. Inorg. Chem. 2012, 5500–5505; d) A. D. Katsenis, R. Inglis, A. Prescimone, E. K. Brechin, G. S. Papaefstathiou, CrystEngComm 2012, 14, 1216–1218; e) J. M. Frost, S. Sanz, T. Rajeshkumar, M. B. Pitak, S. J. Coles, G. Rajaraman, W. Wernsdorfer, J. Schnack, P. J. Lusby, E. K. Brechin, Dalton Trans. 2014, 43, 10690–10694; f) S. Sanz, J. M. Frost, M. B. Pitak, S. J. Coles, S. Piligkos, P. J. Lusby, E. K. Brechin, Chem. Commun. 2014, 50, 3310–3312; g) S. Sanz, J. M. Frost, T. Rajeshkumar, S. J. Dalgarno, G.

Rajaraman, W. Wernsdorfer, J. Schnack, P. J. Lusby, E. K. Brechin, Chem. Eur. J. 2014, 20, 3010–3013.

[17] M. Manoli, R. Inglis, M. J. Manos, V. Nastopoulos, W. Wernsdorfer, E. K. Brechin, A. J. Tasiopoulos, Angew. Chem. Int. Ed. 2011, 50, 4441–4444; Angew. Chem. 2011, 123, 4533.

[18] a) S. R. Drake, A. Lyons, D. J. Otway, D. J. Williams, Inorg. Chem. 1994, 33, 1230–1233; b) S. Wang, Z. Pang, K. D. L. Smith, Y.-S. Yua, C. Deslippe, M. J. Wagner, Inorg. Chem. 1995, 34, 908–917.

[19] N. F. Chilton, R. P. Anderson, L. D. Turner, A. Soncini, K. S. Murray, J. Comput. Chem. 2013, 34, 1164–1175.

[20] A. Escuer, J. Esteban, S. P. Perlepes, T. C. Stamatatos, Coord. Chem. Rev. 2014, 275, 87–129.

[21] W. R. Dunsten, T. A. J. Henry, J. Chem. Soc. 1899, 75, 66–71.

[22] a) G. M. Sheldrick, SHELXTL, Bruker AXS Inc., Madison, WI, USA; b) G. M. Sheldrick, Acta Crystallogr., Sect. A 2008, 64, 112–122.

[23] a) G. M. Sheldrick, SHELXS - A computer program for determination of crystal structures, University of Göttingen, Germany, 1997; b) G. M. Sheldrick, SHELX97 - A program for crystal structure refinement, University of Göttingen, Germany, 1997.

.

538 **Legends to figures**

539

540 **Scheme 1.** R-saloxH2 ligands employed in this work and the modes of coordination of R-saloxH– and
541 R-salox2– in compounds 1–5.
542
543 **Figure 1.** Left: view of the hexanuclear compound 1 (ethanol molecules omitted for clarity). Right:
544 labelled plot of the asymmetric unit of 1. Colour key for all figures: MnII, orange; MnIII dark green;
545 MnIV, firebrick; O, red; N, navy blue; C, black; F, light green.
546
547 **Figure 2.** Hydrogen bonds promoted by the coordinated ethanol molecules in compound 1 (shown as
548 light blue bonds).
549
550 **Figure 3.** Labelled plot of complex 2. For clarity, the coordinated Mesalox2–and MesaloxH– ligands are
551 shown only for one of the manganese atoms.
552
553 **Figure 4.** Labelled plot of the core of complex 3. Hydrogen bonds involving
554 the methanol solvate molecule are indicated as dashed bonds.
555
556 **Figure 5.** Top: view of complex 4. Bottom: labelled plot of the core of complex 4.
557
558 **Figure 6.** View of the hydrogen bonds involving Mn(6), which promotes the 1D arrangement of [Mn12]
559 clusters for complex 4.
560
561 **Figure 7.** Top: view of complex 5 and a labelled plot of its asymmetric unit. Bottom: view of the
562 intermolecular hydrogen bonds (blue bonds).
563
564 **Scheme 2.** Reaction scheme for the syntheses of complexes 1–5. Colour key: MnII, orange; MnIII, dark
565 green; MnIV, firebrick; O, red; N, blue; C, gray; F, light green.
566
567 **Figure 8.** Plot of the MT product vs. T for compound 1. The solid line shows the best fit of the
568 experimental data in the 25–300 K range. Dotted line below 25 K shows the low temperature theoretical
569 simulation. Inset: plot of M vs. T below 100 K showing the unusual maximum of susceptibility.y.
570
571 **Scheme 3.** Coupling schemes for compounds 1 (A and B), 2 (C) and 3 (D).
572

Figure 9. Magnetization plot for complex 1 (●). The solid line shows the first derivative of the magnetization.

Figure 10. Plot of the MT product vs. T for compounds 2 (red circles), 3 (blue squares), 4 (black diamonds) and 5 (green triangles). Inset: magnetization plot for 3. Solid lines show the best fits of the experimental data for 2 and 3.

Figure 11. Plot of the AC M″ for compound 4. Inset: hysteresis cycle measured at 2 K**.**at 2 K..

582 **SCHEME 1**

583

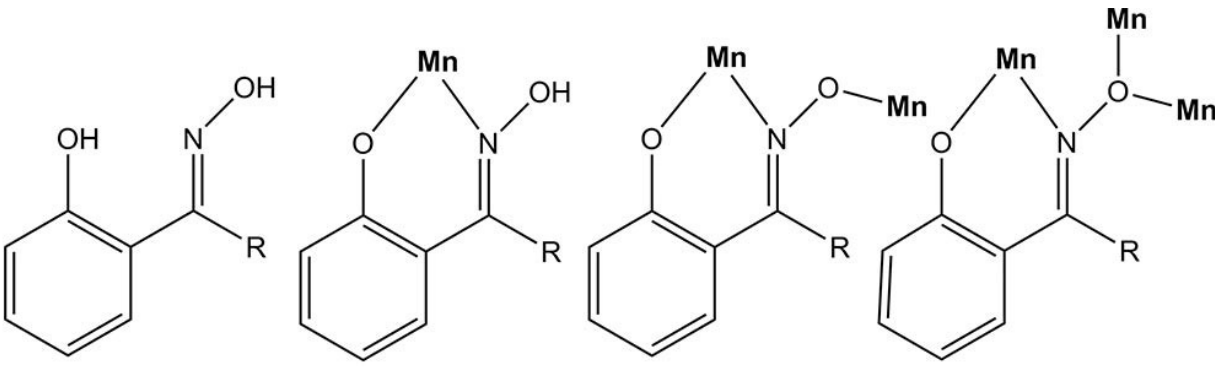

584 R = H, Me, Et

585

586 **FIGURE 1**
587
588

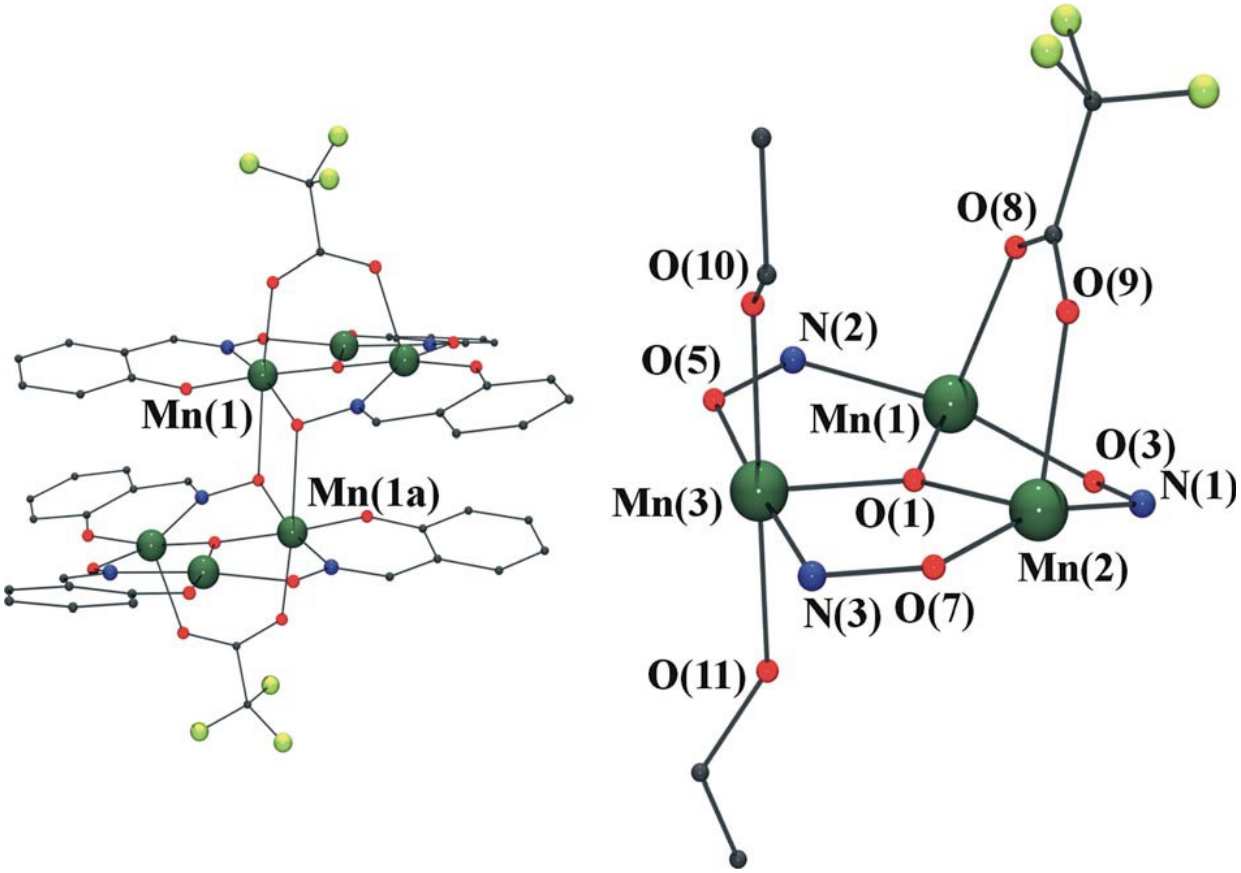

589
590
591

FIGURE 2

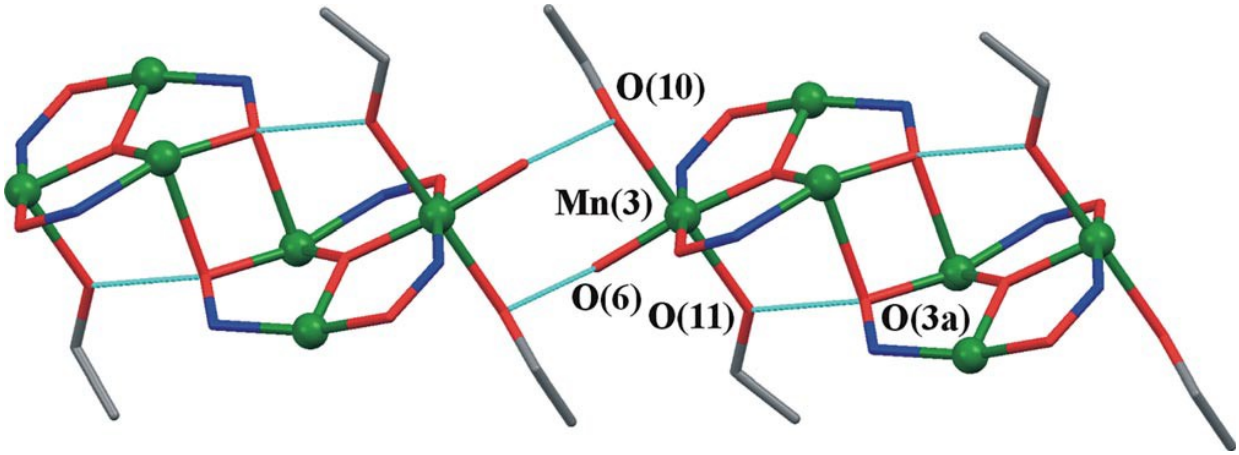

FIGURE 3.

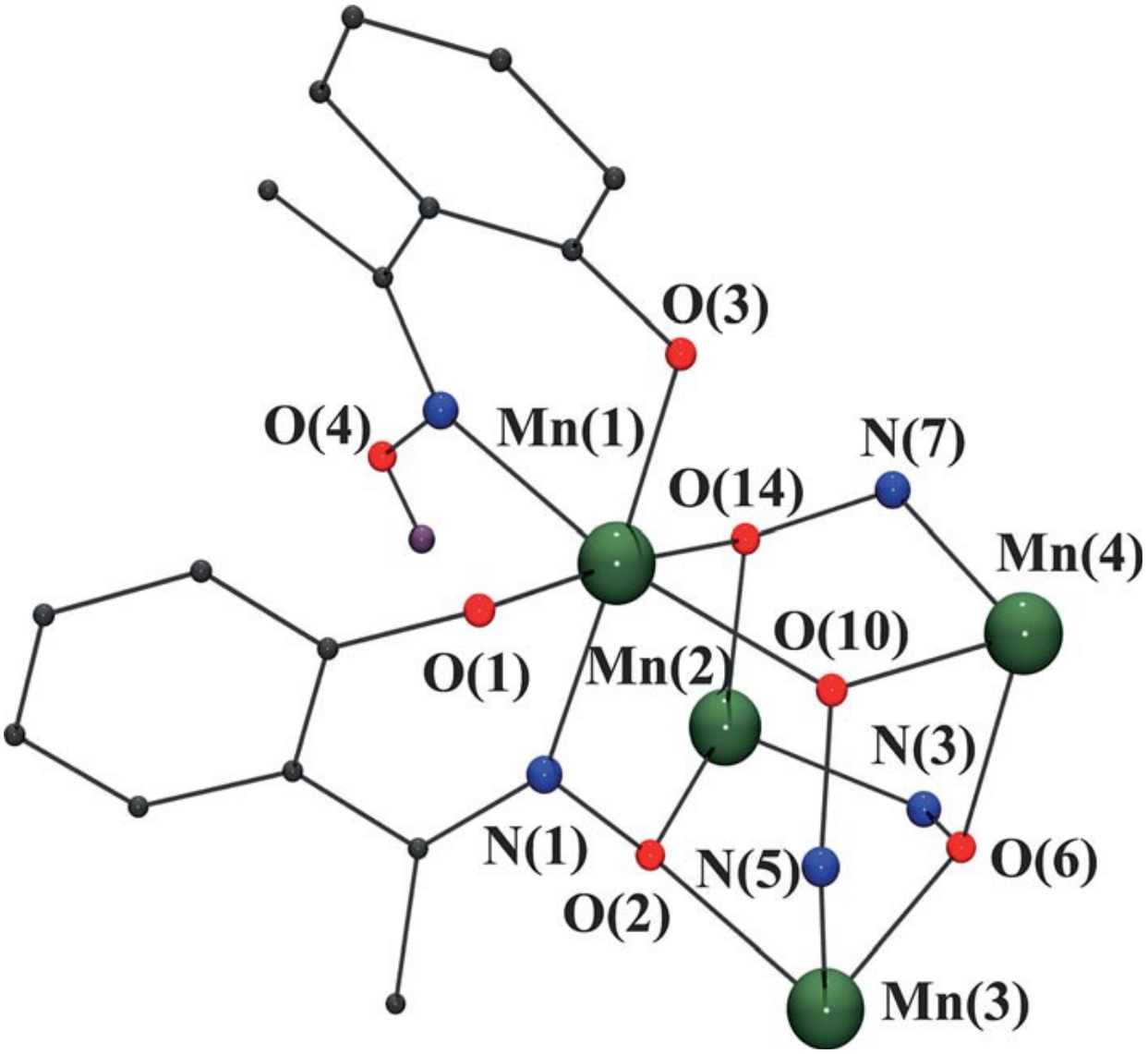

FIGURE 4.

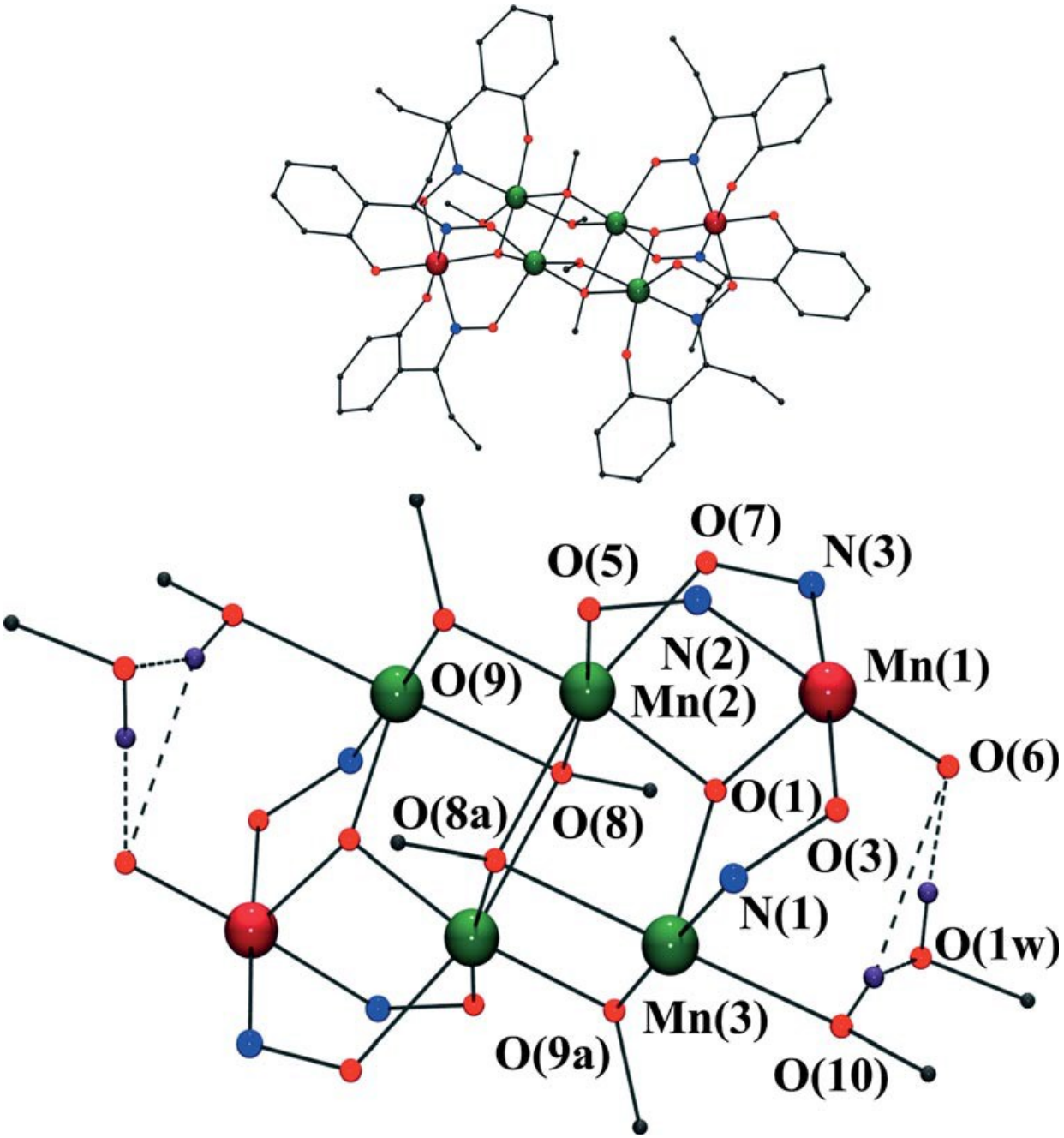

FIGURE 5.

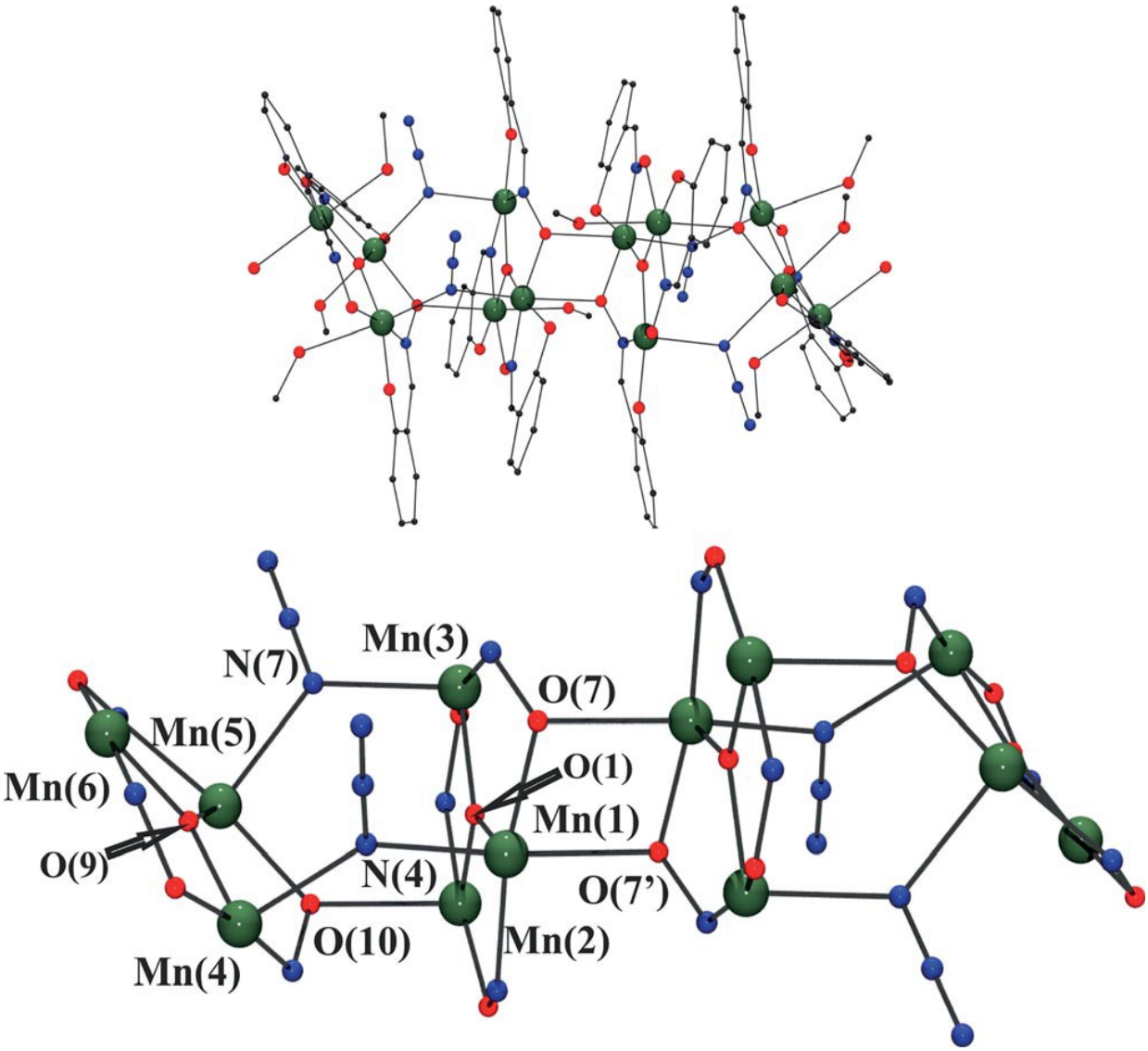

FIGURE 6.

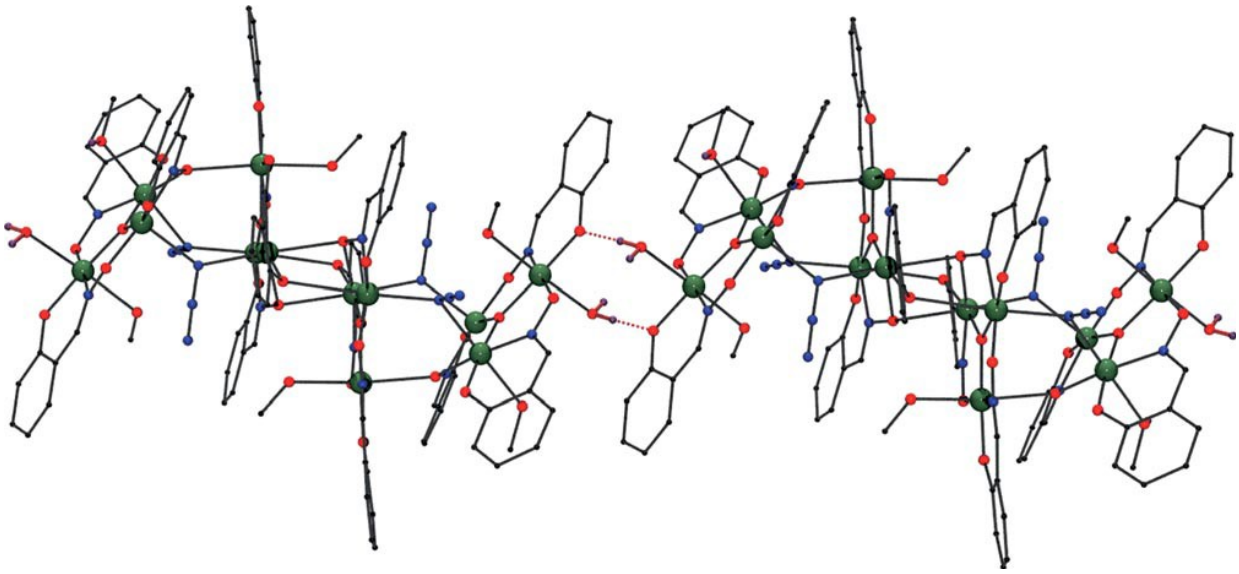

FIGURE 7

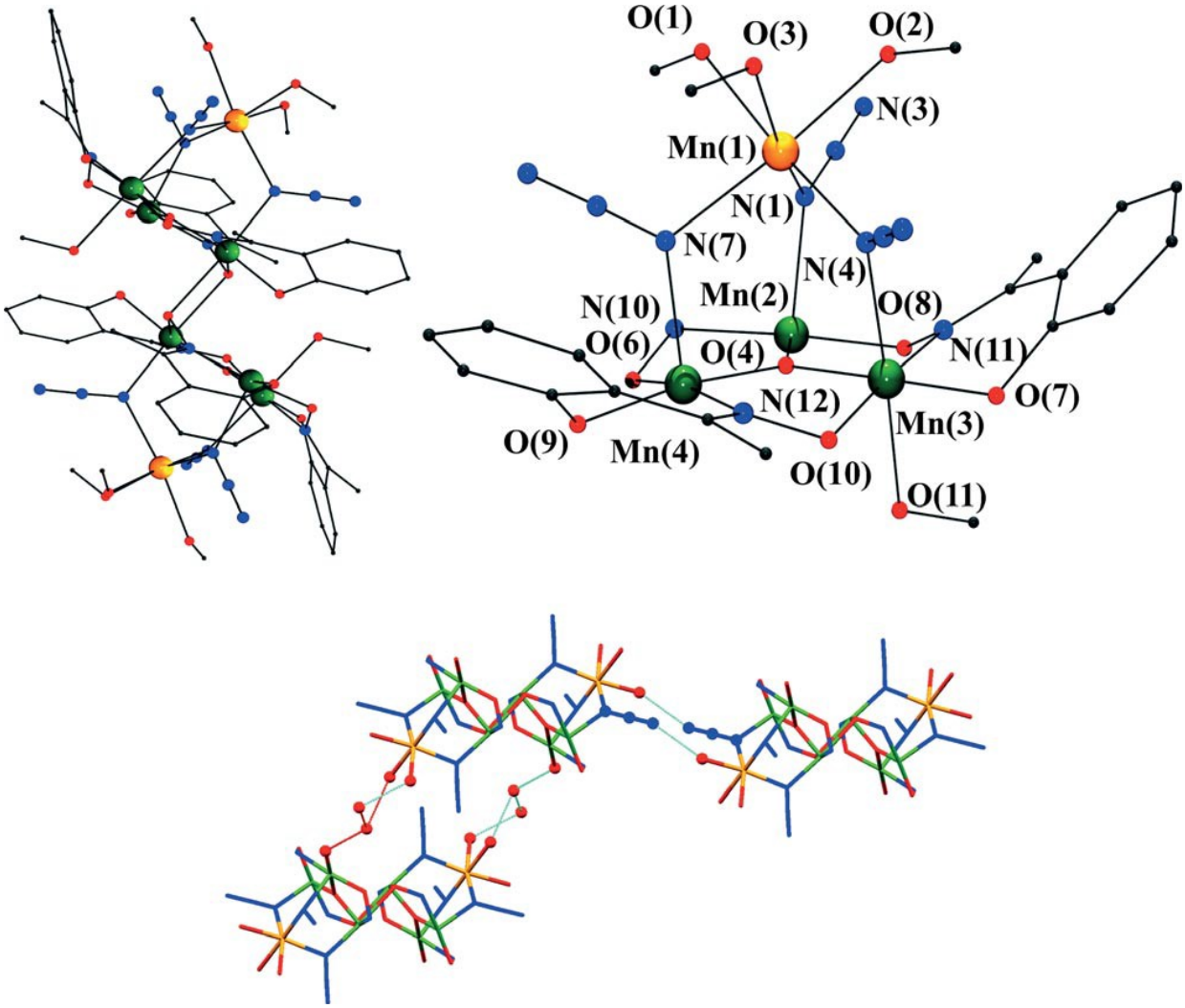
O(1)
O(3)
O(2)
N(3)
Mn(1)
N(1)
N(7)
N(4)
Mn(2)
N(10)
O(8)
O(6)
O(4)
N(11)
N(12)
O(7)
Mn(3)
O(9)
Mn(4)
O(10)
O(11)

SCHEME 2

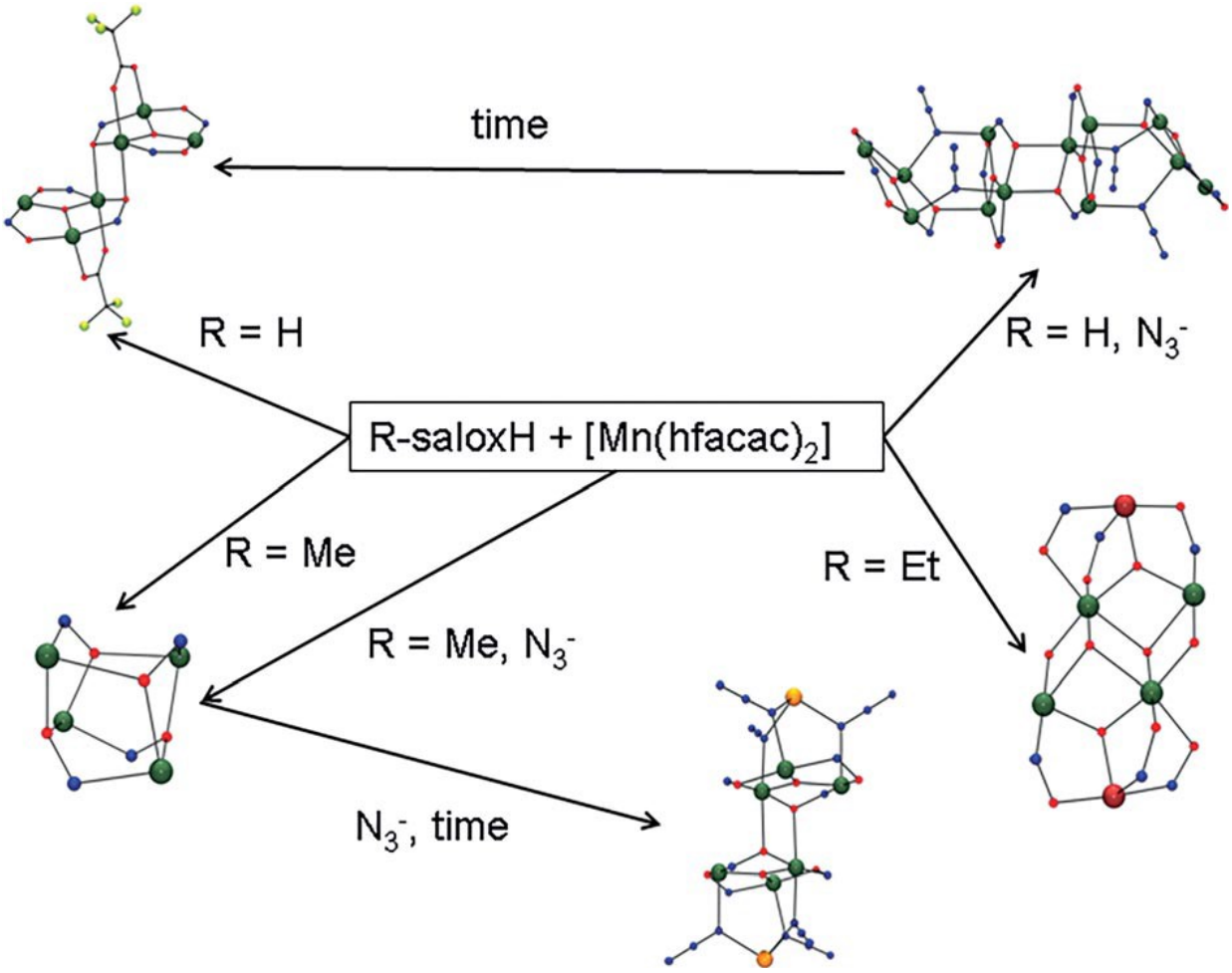

FIGURE 8.

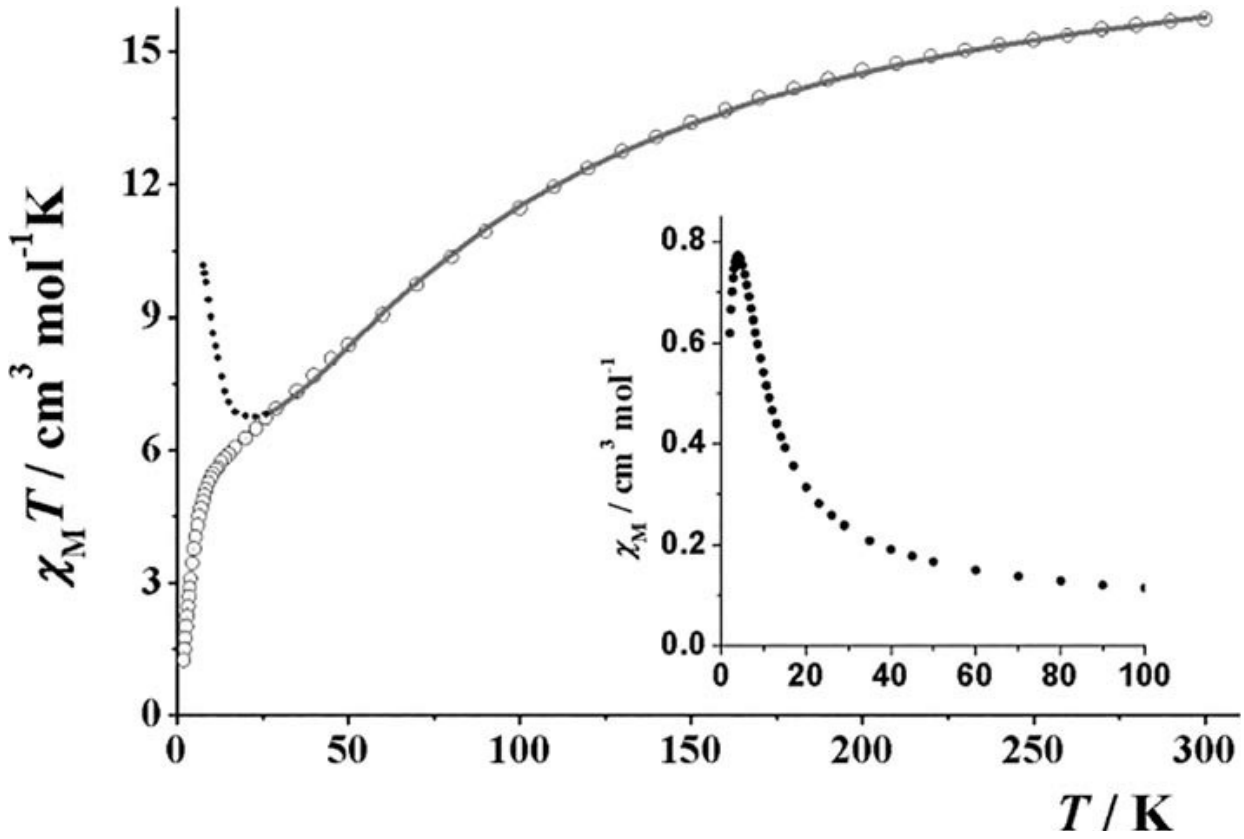
$\chi_M T$ / cm^3 mol^{-1}K
T / K
χ_M / cm^3 mol^{-1}
0
3
6
9
12
15
0
50
100
150
200
250
300
0.0
0.2
0.4
0.6
0.8
0
20
40
60
80
100

SCHEME 3

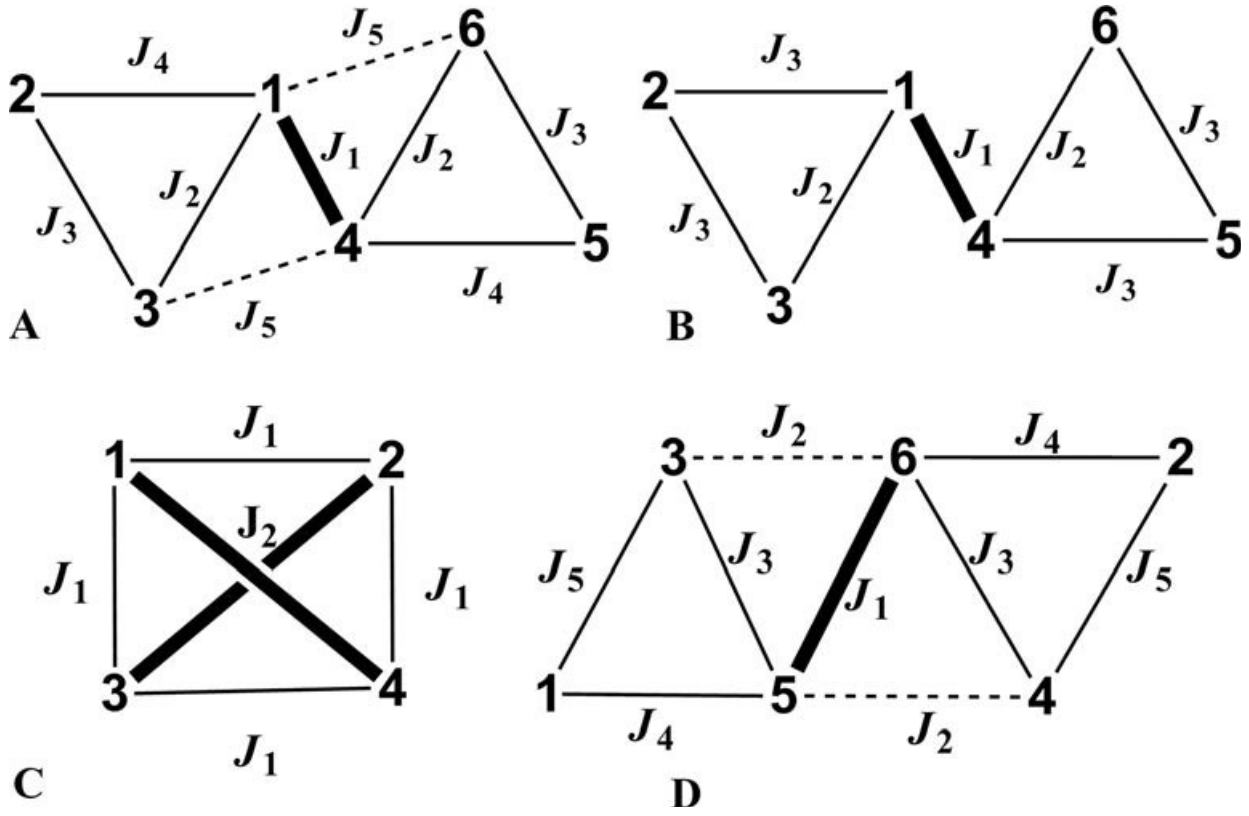

FIGURE 9

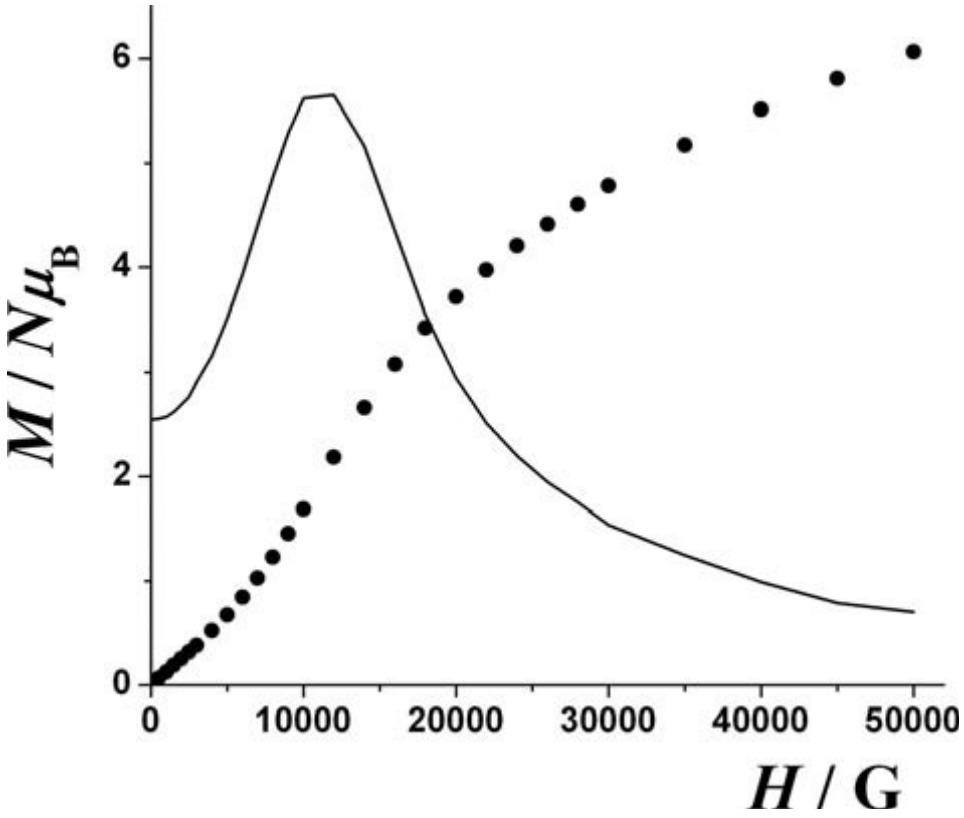

FIGURE 10

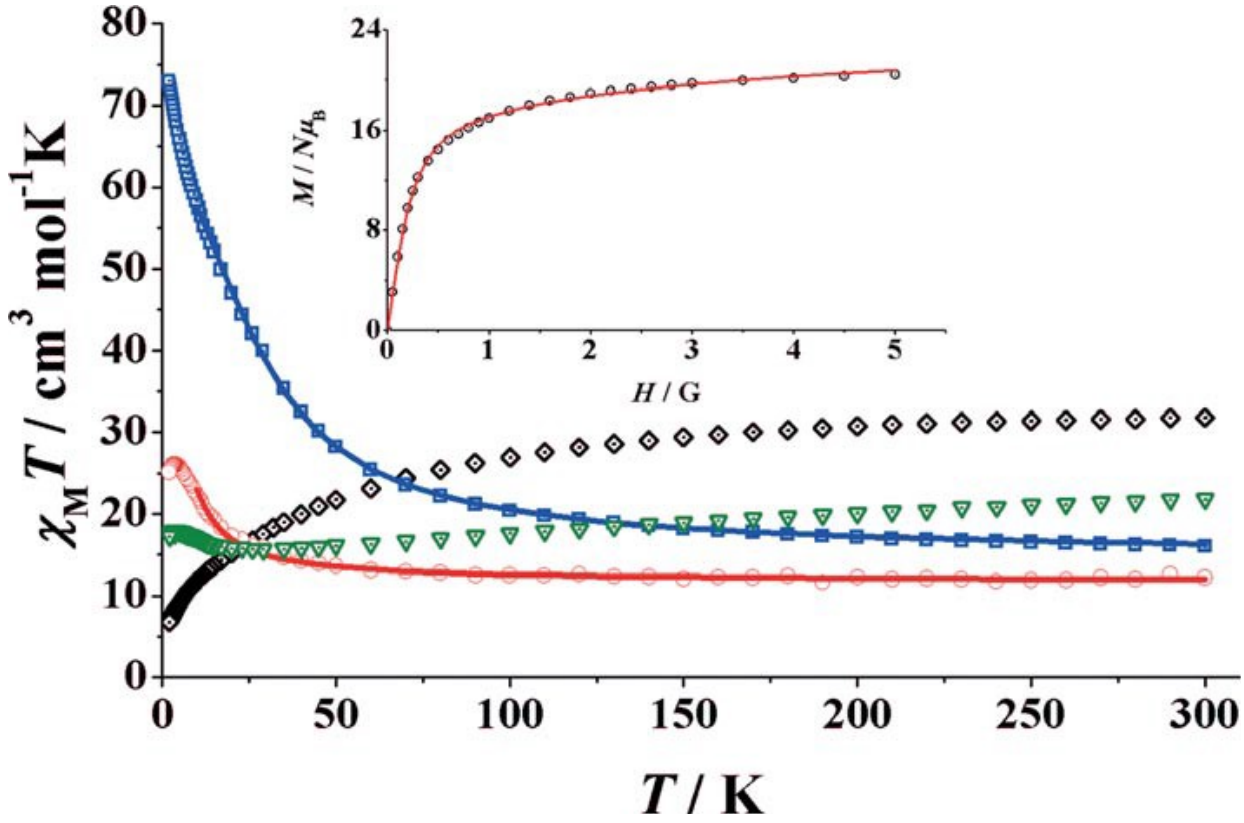
80
70
60
50
40
30
20
10
0
$\chi_M T$ / cm^3 mol^{-1}K
0
50
100
150
200
250
300
T / K
24
16
8
0
$M / N\mu_B$
0
1
2
3
4
5
H / G

FIGURE 11

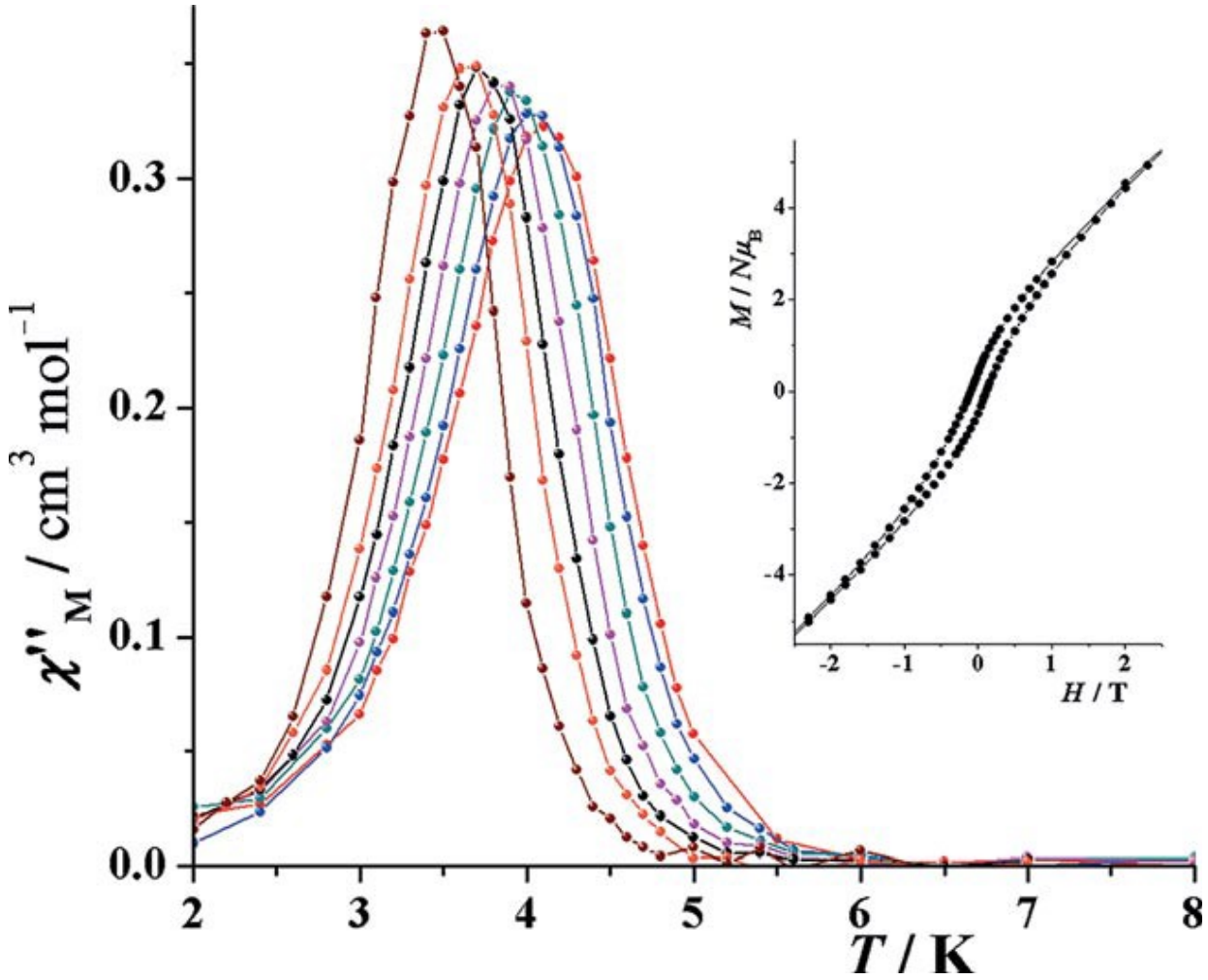

668 **Table 1** BVS data for the oxidation states of the metallic atoms of compounds 1–5.
669

Compound	BVS	Valence	Compound	BVS	Valence
1			**4**		
Mn(1)	3.02	+3	Mn(1)	3.09	+3
Mn(2)	3.03	+3	Mn(2)	3.04	+3
Mn(3)	3.05	+3	Mn(3)	2.99	+3
2			Mn(4)	2.68	+3
Mn(1)	3.09	+3	Mn(5)	3.02	+3
Mn(2)	3.14	+3	Mn(6)	3.28	+3
Mn(3)	3.06	+3	**5**		
Mn(4)	3.18	+3	Mn(1)	1.98	+2
3			Mn(2)	3.11	+3
Mn(1)	3.97	+4	Mn(3)	3.09	+3
Mn(2)	2.94	+3	Mn(4)	3.09	+3
Mn(3)	2.97	+3			

670
671
672
673

Table 2 Selected distances [Å] and angles [°] of the core of compound 1.

Mn(1)–O(1)	1.869(2)	Mn(3)–O(6)	1.880(2)
Mn(1)–O(3)	1.958(2)	Mn(3)–O(10)	2.284(2)
Mn(1)–O(4)	1.862(2)	Mn(3)–O(11)	2.285(2)
Mn(1)–O(8)	2.184(2)	Mn(3)–N(3)	2.003(3)
Mn(1)–O(3a)	2.415(2)		
Mn(1)–N(2)	2.005(2)	Mn(1)–O(1)–Mn(2)	116.2(1)
Mn(2)–O(1)	1.873(2)	Mn(1)–O(1)–Mn(3)	120.6(1)
Mn(2)–O(2)	1.852(2)	Mn(2)–O(1)–Mn(3)	121.3(1)
Mn(2)–O(7)	1.888(2)	Mn(1)–O(3)–Mn(1a)	100.10(8)
Mn(2)–O(9)	2.157(2)	Mn(1)–O(3)–N(1)–Mn(2)	21.4(2)
Mn(2)–N(1)	1.994(3)	Mn(2)–O(7)–N(3)–Mn(3)	14.2(3)
Mn(3)–O(1)	1.878(2)	Mn(3)–O(5)–N(2)–Mn(1)	4.8(3)
Mn(3)–O(5)	1.908(2)	Mn(1a)–O(3)–N(1)–Mn(2)	91.1(2)

679 **Table 3.** Selected distances [Å] and angles [°] of the core of compound 2.
680

Mn(1)–O(1)	1.868(5)	Mn(4)–O(6)	2.234(5)
Mn(1)–O(3)	1.887(5)	Mn(4)–O(10)	1.940(6)
Mn(1)–O(10)	2.241(6)	Mn(4)–O(13)	1.857(6)
Mn(1)–O(14)	1.947(5)	Mn(4)–O(15)	1.895(5)
Mn(1)–N(1)	2.023(6)	Mn(4)–N(7)	1.990(7)
Mn(1)–N(2)	2.254(7)	Mn(4)–N(8)	2.246(6)
Mn(2)–O(2)	1.975(5)		
Mn(2)–O(5)	1.860(5)	Mn(1)–O(14)–Mn(2)	114.8(3)
Mn(2)–O(7)	1.887(6)	Mn(1)–O(10)–Mn(4)	115.7(3)
Mn(2)–O(14)	2.231(6)	Mn(2)–O(2)–Mn(3)	115.4(3)
Mn(2)–N(3)	2.002(8)	Mn(3)–O(6)–Mn(4)	113.9(2)
Mn(2)–N(4)	2.223(6)	Mn(3)–O(2)–N(1)–Mn(1)	78.4(5)
Mn(3)–O(2)	2.236(5)	Mn(2)–O(14)–N(7)–Mn(4)	75.6(5)
Mn(3)–O(6)	1.971(5)	Mn(1)–O(14)–N(7)–Mn(4)	59.5(5)
Mn(3)–O(9)	1.871(5)	Mn(2)–O(2)–N(1)–Mn(1)	59.2(5)
Mn(3)–O(11)	1.898(5)	Mn(1)–O(10)–N(5)–Mn(3)	77.9(6)
Mn(3)–N(5)	2.015(7)	Mn(4)–O(6)–N(3)–Mn(2)	78.6(5)
Mn(3)–N(6)	2.236(8)	Mn(3)–O(6)–N(3)–Mn(2)	57.2(5)
		Mn(4)–O(10)–N(5)–Mn(3)	60.4(6)

681
682
683
684

685 **Table 4**. Selected distances [Å] and angles [°] of the core of compound 3.
686

Mn(1)–O(1)	1.869(1)	Mn(3)–O(8a)	2.265(1)
Mn(1)–O(3)	1.939(1)	Mn(3)–O(9a)	1.973(1)
Mn(1)–O(4)	1.856(1)	Mn(3)–N(1)	1.995(2)
Mn(1)–O(6)	1.888(1)		
Mn(1)–N(2)	2.024(2)	Mn(1)–O(1)–Mn(2)	108.48(6)
Mn(1)–N(3)	2.009(1)	Mn(1)–O(1)–Mn(3)	119.61(6)
Mn(2)–O(1)	1.921(1)	Mn(2)–O(1)–Mn(3)	112.28(6)
Mn(2)–O(5)	1.903(1)	Mn(2)–O(8)–Mn(3a)	97.05(5)
Mn(2)–O(7)	2.137(1)	Mn(2)–O(9)–Mn(3a)	107.27(6)
Mn(2)–O(8)	1.925(1)	Mn(2)–O(8)–Mn(2a)	98.20(5)
Mn(2)–O(9)	1.936(1)	Mn(2)–O(8a)–Mn(3)	88.61(5)
Mn(2)–O(8a)	2.308(1)	Mn(1)–O(3)–N(1)–Mn(3)	47.0(1)
Mn(3)–O(1)	1.926(1)	Mn(2)–O(5)–N(2)–Mn(1)	6.4(1)
Mn(3)–O(2)	1.865(2)	Mn(2)–O(7)–N(3)–Mn(1)	21.0(1)
Mn(3)–O(10)	2.220(2)		

687
688
689

690 **Table 5.** Selected distances [Å] and angles [°] of the core of compound 4.
691

Mn(1)–O(1)	1.877(1)	Mn(5)–O(9)	1.888(1)
Mn(1)–O(2)	1.881(2)	Mn(5)–O(10)	1.970(1)
Mn(1)–O(7)	1.945(2)	Mn(5)–O(12)	1.860(1)
Mn(1)–N(1)	1.988(2)	Mn(5)–O(16)	2.298(2)
Mn(1)–N(4)	2.196(1)	Mn(5)–N(7)	2.295(2)
Mn(1)–O(7)	2.460(1)	Mn(5)–N(11)	2.012(1)
Mn(2)–O(1)	1.874(1)	Mn(6)–N(9)	1.880(1)
Mn(2)–O(3)	1.922(2)	Mn(6)–O(9)	1.880(1)
Mn(2)–O(4)	1.863(1)	Mn(6)–O(13)	1.893(2)
Mn(2)–O(8)	2.260(2)	Mn(6)–O(14)	2.264(2)
Mn(2)–O(10)	2.371(1)	Mn(6)–O(18)	2.314(2)
Mn(2)–N(2)	2.002(2)	Mn(6)–N(12)	2.006(2)
Mn(3)–O(1)	1.870(2)		
Mn(3)–O(5)	1.905(1)	Mn(1)–O(1)–Mn(3)	121.00(7)
Mn(3)–O(6)	1.871(2)	Mn(2)–O(1)–Mn(3)	119.50(7)
Mn(3)–N(3)	2.004(1)	Mn(2)–O(1)–Mn(3)	119.50(7)
Mn(3)–N(7)	2.226(2)	Mn(1)–N(4)–Mn(4)	131.87(8)
Mn(4)–O(9)	1.886(2)	Mn(3)–N(7)–Mn(5)	126.76(8)
Mn(4)–O(11)	1.873(2)	Mn(4)–O(9)–Mn(5)	119.82(7)
Mn(4)–O(15)	1.907(1)	Mn(4)–O(9)–Mn(6)	119.95(7)
Mn(4)–N(4)	2.222(2)	Mn(5)–O(9)–Mn(6)	120.20(7)
Mn(4)–N(10)	2.222(2)	Mn(5)–O(10)–Mn(2)	131.59(7)

692
693
694

695 **Table 6.** Selected distances [Å] and angles [°] for compound 5.
696

Mn(1)–O(1)	2.220(9)	Mn(4)–O(4)	1.855(7)
Mn(1)–O(2)	2.241(9)	Mn(4)–O(6)	1.948(7)
Mn(1)–O(3)	2.204(8)	Mn(4)–O(9)	1.898(7)
Mn(1)–N(1)	2.192(9)	Mn(4)–O(6a)	2.434(8)
Mn(1)–N(4)	2.191(11)	Mn(4)–N(7)	2.176(10)
Mn(1)–N(7)	2.282(9)	Mn(4)–N(12)	2.008(9)
Mn(2)–O(4)	1.887(7)		
Mn(2)–O(5)	1.857(7)	Mn(2)–O(4)–Mn(3)	119.2(4)
Mn(2)–O(9a)	2.563(8)	Mn(2)–O(4)–Mn(4)	121.4(4)
Mn(2)–O(8)	1.913(9)	Mn(3)–O(4)–Mn(4)	119.4(4)
Mn(2)–N(1)	2.257(10)	Mn(1)–N(1)–Mn(2)	119.4(4)
Mn(2)–N(10)	1.968(9)	Mn(1)–N(4)–Mn(3)	117.2(4)
Mn(3)–O(4)	1.877(8)	Mn(1)–N(7)–Mn(4)	117.0(4)
Mn(3)–O(7)	1.882(8)	Mn(4)–O(6)–Mn(4a)	94.9(3)
Mn(3)–O(10)	1.926(7)	Mn(4)–O(6)–N(10)–Mn(2)	39.4(8)
Mn(3)–O(11)	2.328(8)	Mn(3)–O(10)–N(12)–Mn(4)	35.3(8)
Mn(3)–N(4)	2.240(10)	Mn(2)–O(8)–N(11)–Mn(3)	42.3(9)
Mn(3)–N(11)	2.014(9)	Mn(4a)–O(6)–N(10)–Mn(2)	64.8(6)

697
698

699 **Table 7**. Summary of the synthetic conditions for 1–5.
700

	Solvent	Ligand	Base	NaN_3
1·Et_2O	EtOH	SaloxH	Et_3N	no
2	MeOH	MesaloxH	Et_3N	no
3·MeOH	MeOH	EtsaloxH	CsOH	no
4·4MeOH·$2H_2O$	MeOH	SaloxH	Et_3N	yes
5·4MeOH	MeOH	MesaloxH	Et_3N	yes

701
702
703

Table 8. Crystal data and data collection details for the X-ray structure determination of compounds 1–5.

	1	2	3	4	5
Formula	$C_{58}H_{64}F_6Mn_6N_6O_{23}$	$C_{64}H_{60}Mn_8N_8O_{16}$	$C_{61}H_{78}Mn_6N_6O_{21}$	$C_{94}H_{108}Mn_{12}N_{24}O_{42}$	$C_{60}H_{66}Mn_8N_{24}O_{26}$
M_r	1644.70	1416.96	1560.93	2905.32	2003.05
System	triclinic	monoclinic	triclinic	triclinic	triclinic
Space group	$P\bar{1}$	$P2_12_12_1$	$P\bar{1}$	$P\bar{1}$	$P\bar{1}$
a [Å]	11.271(4)	13.428(3)	11.255(4)	12.2924(4)	11.688(5)
b [Å]	12.131(3)	15.715(4)	12.442(2)	14.1267(4)	12.886(5)
c [Å]	14.131(3)	29.525(7)	12.670(3)	18.9933(6)	15.451(6)
α [°]	80.31(2)	90	80.26(2)	85.301(1)	92.658(5)
β [°]	72.83(2)	90	89.49(2)	73.171(1)	111.182(5)
γ [°]	86.46(2)	90	88.34(2)	66.240(1)	106.349(5)
V [Å^3]	1829.0(9)	6230(3)	1747.9(8)	2912.9(2)	2053(1)
Z	1	4	1	1	1
T [K]	293(2)	100(2)	105(2)	100(2)	100(2)
λ(Mo-K_α) [Å]	0.71073	0.77490	0.71073	0.77490	0.77490
$P_{calcd.}$ [g cm^{-3}]	1.493	1.511	1.483	1.656	1.618
μ(Mo-K_α) [mm^{-1}]	1.093	1.092	1.125	1.697	1.614
R	0.0525	0.0543	0.0328	0.0280	0.0923
ωR^2	0.1663	0.1194	0.0938	0.1107	0.2530

710